Obtaining the caloric curve from collisions

A. Chernomoretz,[1] C. O. Dorso,[1] and J. A. López[2]
[1]*Departamento de Física, Facultad de Ciencias Exactas y Naturales, Universidad de Buenos Aires, Nuñez 1428, Buenos Aires, Argentina*
[2]*Department of Physics, University of Texas at El Paso, El Paso, Texas 79968*
(Received 13 January 2001; published 20 September 2001)

It might be possible that thermodynamic properties of nuclear matter, such as the caloric curve, could be obtained from heavy-ion reactions. Recent experimental and computational studies of nuclear experiments have obtained contradictory caloric curves for nuclear matter. This work improves on previous theoretical studies by considering the fragmentation produced by collisions, and introducing the methodology needed to identify the fragments, their temperature, energy, and a caloric curve. The main findings are the crucial reduction of energy produced in the promptly emitted particles, the existence of a well-defined fragmentation time, the connection of the temperature of the detected fragments with that at fragmentation time, and the possibility of obtaining the caloric curve from collisions.

DOI: 10.1103/PhysRevC.64.044605 PACS number(s): 24.10.Lx, 25.70.Pq, 25.70.Mn, 65.20.+w

I. INTRODUCTION

Nuclear collisions at energies in the hundreds of MeV's produce excited systems which break into several medium-size fragments [1]. This multifragmentation phenomena, similar to what happens in inertial confinement reactors [2] and in the synthesis of nanostructure surfaces [3], could be the adaptation of a macroscopic phase transition to a small and transient many-body system.

In the field of nuclear physics, the possibility of achieving critical behavior in heavy-ion collisions has attracted a lot of attention. This interest on critical exponents was triggered by the seminal study of critical phenomena in proton-Xe and proton-Ar collisions of the Purdue group [4,5] and then undertaken by other groups [6]. More recently, modern detection technology has made possible the experimental determination of the caloric curve [7,8], i.e., the relation between the system's temperature and its excitation energy at fragmentation time. The procedures used, however, present several complications due mainly to the finite size of the system, its transient nature, and the limitation of obtaining nothing more than the final fragments from the reaction.

As explained by Pochodzalla and Trautmann in Ref. [9], there are complications, for instance, in the reconstruction of the energy deposition starting from the exit channels, and, thus, in the calculation of the caloric curve. Other difficulties come from the variation of the size of the systems produced in the reactions [10], side feeding affecting the final mass distribution [11], and on the use of final spectra which have been necessarily modified by the natural evolution of the reaction [12].

Indeed, experiments using different ''thermometers'' have led to contradictory caloric curves that go from the typical ''rise-plateau-rise'' pattern [13], to a more peculiar ''rise-plateau'' behavior [14,15], and yet to a ''rise-rise'' shape without the characteristic plateau of first-order phase transitions [16,17]. The suppression of the final temperature rise could be related to a presumably low breakup density [18], or to an increased fragmentation at high excitation energies that depletes the heat-storing medium-size fragments [9].

With so many variables affecting the determination of the caloric curve of nuclear matter, the question to answer is then, is it at all possible to extract the caloric curve from nuclear collisions? Recently this question was addressed in a molecular dynamics study for a nuclearlike system in a container [19], and for a freely expanding classical system [22].

Although the two calculations are not directly comparable, not among themselves nor to experiments, both exercises were able to obtain a caloric curve. Sugawa and Horiuchi [19], using an antisymmetrized molecular dynamics, studied a contained uniformly excited system with a fixed pressure, and obtained a raise-plateau-raise caloric curve. On the other hand, Strachan and Dorso [22] used a classical, uniformly excited, Lennard-Jones system freely expanding into space to obtain a caloric curve with a raise-plateau shape. The difference between these results comes from the collective expansion present in free finite systems (but not on infinite or contained systems), which acts as an energy sink and limits the temperature rise [22].

Independent of their differences, these exercises appear to underline the fact that small breaking systems can yield information about the caloric curve. But in view of the crucial role played by the geometrical aspects of the breaking system, i.e., contained vs freely expanding systems, a refined question to ask would then be, what is the role played by the collision on the obtention of the caloric curve? In other words, would the strong correlations induced by the highly nonlinear dynamics of the collision impede the obtention of the caloric curve? A calculation more closely matching the experimental collisions is what motivates the present study.

This work uses the numerical weaponry developed in Ref. [22] to focus on systems that are excited via the collision with energetic projectiles, and, again, our main objective is the determination of the caloric curve. The paper is organized as follows. After describing the model used and the fragment-recognition algorithms in Sec. I, Sec. II describes typical time evolutions of the fragmenting systems and the characteristic time scales. Section III proposes a way to calculate the effective excitation energy of the fragmenting system, and Sec. IV studies the effective temperature of the

fragmenting system and resulting clusters. The resulting caloric curve is presented in Sec. V, and some concluding remarks close the paper in Sec. VI.

II. THE MODEL

Due to the complications of the breakup process, a complex model with proper auxiliary tools is needed. To begin with, the evolution of the collision is modeled with a molecular dynamics (MD) code, but since MD operates at the ''nucleon'' level, it is necessary to transform the particle information into fragment information by means of a fragment-recognition algorithm. Furthermore, to use the caloric curve as a signature of a phase transition, the time at which the system fragments must be determined using a quantity known as the partition ''persistence.''

A. The molecular dynamics model

The virtues of molecular dynamics for the study of nuclear collisions have been stated elsewhere [20]. As was mentioned in the Introduction here we study the behavior of a two-dimensional system composed by classical particles that interact via a two-body Lennard-Jones potential:

$$V(r)=4\epsilon\left[\left(\frac{\sigma}{r}\right)^{12}-\left(\frac{\sigma}{r_{cut}}\right)^{12}-\left(\frac{\sigma}{r}\right)^{6}+\left(\frac{\sigma}{r_{cut}}\right)^{6}\right], \qquad (1)$$

where r_{cut} is the cutoff radius, and the potential is taken as zero for $r \geqslant r_{cut}$. We consider $r_{cut}=3\sigma$. The units of time and energy are $t_0=\sqrt{\sigma^2 m/48\epsilon}$ and ϵ, respectively.

This work studies the time evolution of numerical simulations of head-on projectile-target collisions. The target consists of a randomly oriented two-dimensional (2D) drop of 100 particles on its ''ground state,'' $\epsilon_0 \sim -2.8\epsilon$. The projectile is a randomly oriented three-particle drop boosted into the target at different energies. The numerical integration of the equations of motion is performed with a velocity-Verlet algorithm with a time step of $t_{int}=0.0025t_0$ assuring an energy conservation better than 0.05%. Figure 1 shows an evolution corresponding to a typical collision experiment.

The range of kinetic projectile energies considered goes from $E_{beam}=18\epsilon$ to 2520ϵ in the center of mass reference frame with 200 collisions performed for each energy. Studying such a rather broad energy range, quite different types of dynamical evolutions are found: from events in which the projectile is adsorbed by the droplet surface, up to events where a mass spectrum with an exponential decay is observed. As can be seen in Fig. 2, U-shaped and power-law-like mass spectra are observed for intermediate energies.

B. Fragment recognition

To obtain fragment information, the complete microscopic ''nucleon'' data resulting from MD must be analyzed using fragment-recognition algorithms. Many such algorithms exist; the ones used here are described next.

The simplest and more intuitive cluster definition is based on correlations in configuration space: a particle *i* belongs to a cluster *C* if there is another particle *j* that belongs to *C* and

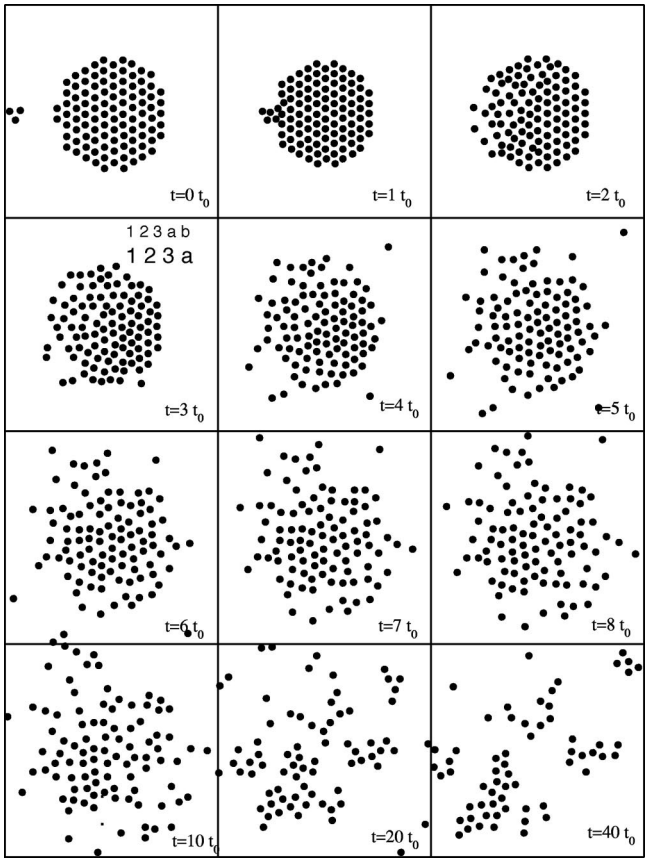

FIG. 1. Snapshot sequence of the dynamical evolution of a typical $E_{beam}=1120\epsilon$ experiment.

$|\mathbf{r_i}-\mathbf{r_j}| \leqslant r_{cl}$, where r_{cl} is a parameter called the clusterization radius. If the interaction potential has a cutoff radius r_{cut}, then r_{cl} must be equal to or smaller than r_{cut}; in this work $r_{cl}=r_{cut}=3\sigma$. The algorithm that recognizes these clusters is known as the ''minimum spanning tree'' (MST). The main drawbacks of this method is that only correlations in **r** space are used, neglecting completely the effect of momentum. The MST clusters give incorrect information when the system is still dense, and are meaningful only late in the evolution when the system is a dilute mixture of free particles and cool fragments.

An extension of the MST is the ''minimum spanning tree in energy'' (MSTE) space algorithm. In this case, a given set of particles $i,j,\ldots,k$, belongs to the same cluster C_i if

$$\forall\ i \epsilon C_i, \quad \exists\ j \epsilon C_i / e_{ij} \leqslant 0, \qquad (2)$$

where $e_{ij}=V(r_{ij})+(\mathbf{p}_i-\mathbf{p}_j)^2/4\mu$, and μ is the reduced mass of the pair $\{i,j\}$. MSTE searches for configurational correlations between particles considering the relative momenta of particle pairs. In spite of not being supported by a physically sound definition of a cluster, the MSTE algorithm typically recognizes fragments earlier than MST. Furthermore, due to its sensitivity in recognizing promptly emitted particles, it is extremely useful to study the preequilibrium energy distribution of the participant particles.

A more robust algorithm is based on the ''most bound partition'' (MBP) of the system [23]. The MBP is the set of

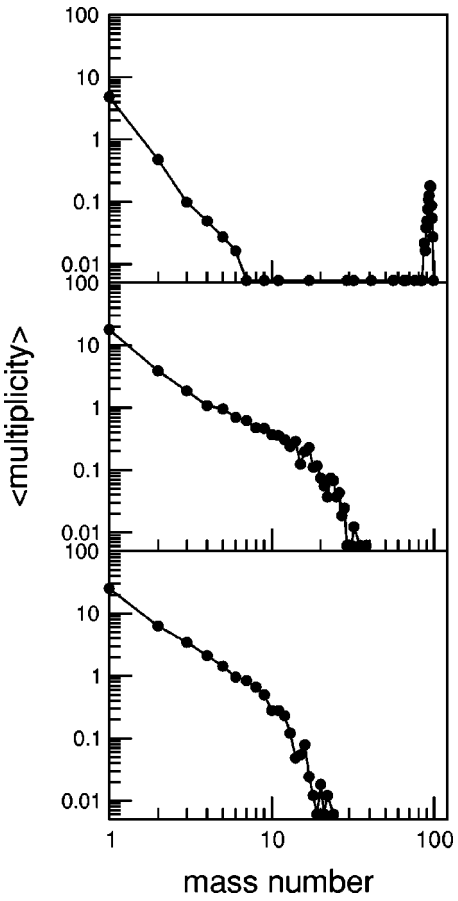

FIG. 2. Asymptotic mass spectra corresponding to $E_{beam}=280\epsilon$, 1120ϵ, and 2520ϵ from top to bottom, respectively.

clusters $\{C_i\}$ for which the sum of the fragment internal energies attains its minimum value:

$$\{C_i\}=\underset{\{C_i\}}{\text{argmin}}\left[E_{\{C_i\}}=\sum_i E_{int}^{C_i}\right],$$

$$E_{int}^{C_i}=\sum_i\left[\sum_{j\in C_i}K_j^{\text{c.m.}}+\sum_{\substack{j,k\in C_i\\ j\leqslant k}}V_{j,k}\right], \tag{3}$$

where the first sum in Eq. (3) is over the clusters of the partition, $K_j^{\text{c.m.}}$ is the kinetic energy of particle j measured in the center of mass frame of the cluster which contains particle j, and V_{ij} stands for the interparticle potential. It can be shown that clusters belonging to the MBP are related to the most-bound density fluctuation in **r**-**p** space [23].

The algorithm that finds the MBP is known as the ''early cluster recognition algorithm'' (ECRA). Since ECRA searches for the most-bound density fluctuations in **r**-**p** space, valuable space and velocity correlations can be extracted at all times, especially at the very early stages of the evolution. This has been used extensively in many fragmentation studies [20–25] and has helped to discover that excited drops break very early in the evolution.

The performance of these three fragment-recognition methods (MST, MSTE, and ECRA) has been illustrated before [22–24], with the general feature that partitions obtained by ECRA stabilize very early in time, much earlier than those of MST and MSTE. As expected, at asymptotic times all three algorithms give the same results.

C. Partition persistence

As stated in the Introduction we consider the caloric curve as the functional relationship between the excitation energy of the system and its temperature *at fragmentation time*. Therefore, we need to estimate the system's excitation energy and temperature when the breakup occurs. In order to do that, the fragment-formation time, τ_{ff}, can be defined as the time in which the system breaks in a definite way; that is, after τ_{ff} the fragments might just evaporate only a few monomers. To estimate τ_{ff} it is necessary to measure the similitude between partitions at different times; this can be achieved with the ''microscopic persistence coefficient,'' P [25]:

$$P[X,Y]=\frac{1}{\sum_{cl}{n_i}}\sum_{cl}n_i\frac{a_i}{b_i}, \tag{4}$$

where $X\equiv\{C_i\}$ and $Y\equiv\{C_i'\}$ are two different partitions, b_i is the number of pairs of particles in the cluster C_i of partition X, a_i is the number of pairs of particles that belong to cluster C_i and also are together in a given cluster C_j' of partition Y, and n_i is the number of particles in cluster C_i. $P[X,Y]$ is equal to 1 if the microscopic composition of the partition X equals that of Y, and it tends to 0 when none of the constituent particles of a given cluster in X appear together in any cluster in Y.

It is useful to study the time evolution of the quantities

$$\hat{P}^+[X(t)]\equiv\langle P[X(t),X(t\rightarrow\infty)]\rangle_{events},$$

$$\hat{P}^-[X(t)]\equiv\langle P[X(t\rightarrow\infty),X(t)]\rangle_{events},$$

$$\hat{P}^{dt}[X(t)]\equiv\langle P[X(t),X(t+dt)]\rangle_{events}, \tag{5}$$

where $X(t)$ represents a partition calculated at time t, $X(t\rightarrow\infty)$ is a partition at asymptotic times, and $\langle\cdots\rangle_{events}$ represent an average over the whole set of collisions. Simply stated, $\hat{P}^+[X(t)]$ determines if the particles that are together at time t remain together asymptotically. Likewise, $\hat{P}^-[X(t)]$ measures the reciprocal value, i.e., the degree in which the asymptotic partition is contained in the one at time t. Together, $\hat{P}^+$ and $\hat{P}^-$ can be used to analyze how the microscopic composition of the system's most-bound partition evolves towards its asymptotic form. Finally $\hat{P}^{dt}[X(t)]$ gives an idea of the *activity* of the partition analyzed, and thus can be used to define a fragment-formation time, τ_{ff}, once a certain degree of stabilization is achieved.

Instead of the straightforward use of the quantities introduced in Eq. (5) we found it worthy to analyze the respective normalized quantities:

$$P^+[X(t)]\equiv\hat{P}^+[X(t)]/\langle P[X(t\rightarrow\infty),X'(t\rightarrow\infty)]\rangle_{events},$$

$$P^{-}[X(t)] \equiv \hat{P}^{-}[X(t)] / \langle P[X(t), X'(t)] \rangle_{events},$$

$$P^{dt}[X(t)] \equiv \hat{P}^{dt}[X(t)] / \langle P[X(t+dt), X'(t+dt)] \rangle_{events}, \quad (6)$$

where X' stands for a partition composed by the same clusters of partition X, but each fragment has one particle evaporated. This normalized quantities compare the actual value of $\hat{P}$'s to an evaporativelike reference level. P^{+}, P^{-}, and P^{dt} allow us to estimate the time at which microscopic stability is achieved (i.e., the fragment-formation time), and will be referred to as the forward, backward, and differential persistence coefficients, respectively.

III. DYNAMICAL EVOLUTION

Armed with the tools presented before (MD, MST, MSTE, and ECRA, and P^{+}, P^{-}, and P^{dt}) we now proceed to study the dynamical evolution of the collisions described in Sec. II A. Analyzing the projectile-target momentum transfer allows the characterization of the collision into stages and the identification of promptly emitted particles. This in turn makes possible the study of the time evolution of the excitation energy and the determination of the fragment-formation time.

A. Collision stages

Two stages are seen in the collisions studied, an ordered initial highly collisional stage produced when the projectile hits the drop surface, and a disordered chaotic collision pattern that distributes the energy. The ordered collisions of the first stage form a shock wave responsible for a rapid emission of energetic light particles from the surface. As this wave travels through the drop, it produces density fluctuations and internal fractures while it transfers momentum and initiates the disordered collisions that thermalize the excitation.

To get a deeper understanding of this process we calculate the ''mean velocity transfer,'' defined as

$$M_j(t) = \left\langle \sum_{i=0}^{N} \left| [\vec{v}_i(t+dt) - \vec{v}_i(t)] \cdot \hat{e}_j \right| \right\rangle_{events},$$

where j denotes the incident (x) and perpendicular (y) directions, $dt = 0.25$, and $\hat{e}_j$ is a unit vector in the x or y directions. Figure 3 shows the temporal evolution of M_x and M_y for projectile energy $E_{beam} = 280\epsilon$, 630ϵ, 1120ϵ, and 1750ϵ. In all cases $M_x > M_y$ at the first stage of the collision, as expected from the centrality of the collisions. The maximum value of M_x and M_y is simultaneously attained at $t \sim 2t_0 - 3t_0$, when the shock front reaches the middle region of the drop and more particles are involved in the momentum transference process. At $t \sim 4t_0 - 7t_0$ the shock wave has crossed the drop and $M_x \sim M_y$ for the whole range of energies considered; at this time the memory of the entrance channel is lost.

The isotropic collisions (*disordered collisional mode*) are responsible for the momentum redistribution among the particles remaining in the system. This energy heats up the system and builds a collective expansive motion. The disordered collisional mode is the only one present in uniformly excited systems where it is responsible for the production of fragments and their outward flux that spread them into space [22,23].

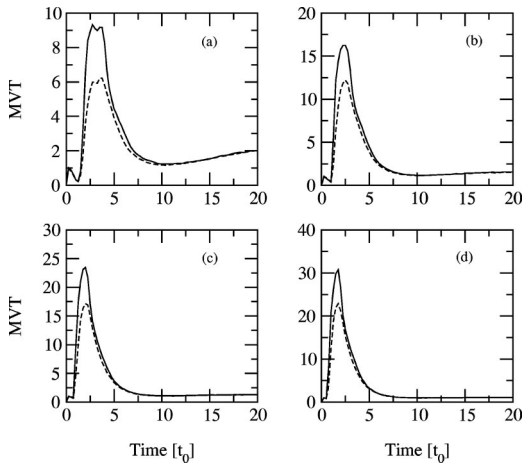

FIG. 3. Mean velocity transfer coefficients, M_x (solid lines) and M_y (dashed lines), are shown for beam energies $E_{beam} = 280\epsilon$ (a), 650ϵ (b), 1120ϵ (c), and 1800ϵ (d). The maximum value is achieved approximately when the shock front reaches the middle of the drop. $M_x > M_y$ reflects the symmetry of the collision, and $M_x \sim M_y$ is a signal of an isotropic collision pattern.

The MSTE algorithm can be used to study the size of the biggest MSTE cluster, the total multiplicity, and the persistence coefficients. Figures 4(a)–4(c) show the time evolution of these three quantities. The picture emerging indicates that, due to the violent initial collision, some particles acquire a lot of kinetic energy which prevents them from being a part of the biggest fragment, albeit of being configurationally close to it or even inside. This reduces the mass of the biggest MSTE fragment in this early stage (up to $t \sim 3t_0$), and increases the total multiplicity. This trend is sustained until the average momentum per particle allows the particles that are configurationally close to be bound. After the initial reduction of the fragment size, there is a coalescencelike behavior that makes the partition multiplicity shrink and the biggest cluster grow until it reaches a maximum at $t \approx 7t_0$. This time marks the end of the initial energy deposition process and in what follows, it will be referred as the *deposition time*, t_d.

The persistence coefficients (6) can be used to understand how the partition reaches its microscopic composition at asymptotic times. Figure 4(c) shows the temporal evolution of $P^{+}[X(t)]$ and $P^{-}[X(t)]$ calculated using MSTE partitions for $E_{beam} = 1120\epsilon$ and using $t_{\infty} = 50t_0$. The backward persistence coefficient shows an initial steep decrease, corresponding to a fragment production stage, followed by a subsequent increase due to a reabsorptionlike dynamics that subsists up to t_d. (Remember that high P^{-} values indicate that more particles that belong to a given asymptotic cluster are together at time t.) Consistently, the P^{+} coefficient shows a plateau during this reabsorption stage that also extends up to t_d, followed then by a monotonic increase due to an evaporationlike dynamics of the MSTE clusters. During this stage

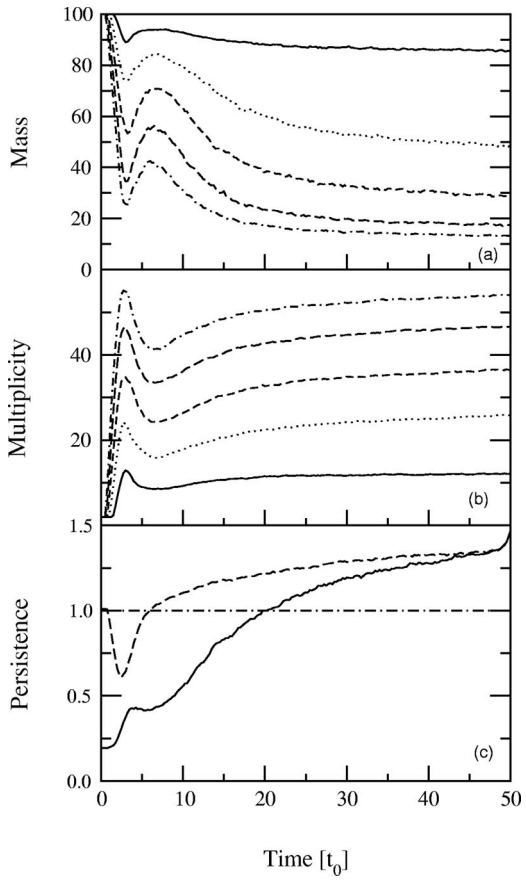

FIG. 4. Mass of the biggest MSTE cluster (a) and the multiplicity of MSTE fragments (b) for $E_{beam}=280\epsilon$ (solid lines), $E_{beam}=630\epsilon$ (dotted lines), $E_{beam}=1120\epsilon$ (dashed lines), $E_{beam}=1750\epsilon$ (long-dashed lines), and $E_{beam}=2520\epsilon$ (dot-dashed lines). (c) shows the forward persistence coefficient P^+ (solid lines) and the backward persistence coefficient P^- (dashed lines) for MSTE partitions for $E_{beam}=1120\epsilon$ experiments.

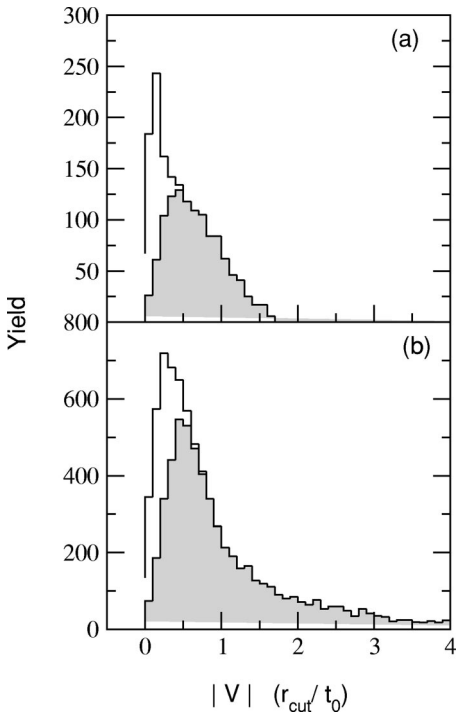

FIG. 5. Histograms of the asymptotic velocity modulus for monomers calculated for $E_{beam}=280\epsilon$ and 2520ϵ. The solid outline transparent histogram corresponds to counts produced by the complete set of asymptotic monomers; the gray histogram corresponds to counts produced by the promptly emitted ones.

of the evolution, the MST algorithm identifies one large cluster with $\sim$80%–90% of the mass of the system, revealing that the system is still dense.

In summary, there is an initial stage (lasting up to $t\sim 3t_0$) characterized by the existence of an ordered shock wave (with $M_x > M_y$) which expels light particles from the surface, reduces the biggest fragment, and increases multiplicity (i.e., decreases P^-). At $t\sim 4t_0-7t_0$ the wave has crossed the drop distributing the energy uniformly ($M_x \sim M_y$) and a coalescencelike behavior sets in (as seen by a rise of P^-) washing out the memory of the entrance channel, reducing the partition multiplicity, and enlarging the biggest cluster up to $\sim$80%–90% of the total mass. This is finally followed by an evaporationlike dynamics of the clusters as indicated by a monotonic increase of P^+.

B. PEP's and excitation energy

As in the experimental case [17], the observed presence of promptly emitted particles (PEP's) makes it impossible to know *a priori* how much of the beam energy is used as excitation energy. This complication, conspicuously absent in calculations of contained or infinite systems, demands a sensible definition of the excitation energy which necessarily should depend on the PEP's.

The PEP's can be defined as those unbound light clusters (mass $\leqslant 4$) detected by the MSTE algorithm at time t_d and that remain unbound at any later time (i.e., no reabsorption). The number of PEP's can be quantified as in Fig. 5 which shows the velocity distribution of monomers for beam energies 280ϵ and 2520ϵ. The histograms show the asymptotic velocity distributions calculated for all monomers (solid outline transparent histogram) and for PEP monomers only (gray histogram). PEP's account for most of the monomer production and for the large velocity asymmetry observed at both beam energies.

With the PEPs defined, their kinetic energy can be used to estimate the energy that remains in the system. Figures 6(a) and 6(b) show the energy carried by the PEP's and the number of PEP's as a function of the beam energy, respectively. With the number of PEP's and their energy quantified, the energy that remains in the system after t_d can also be obtained. Figure 6(c) shows the excitation energy of the target, E^*, as a function of the beam energy. These figures show that the fraction of the available energy that leaves the system as a consequence of this early emission is considerable. Moreover, the excitation energy shows a saturation behavior indicating that there is a limit in the amount of energy that can be transferred in a collision, an effect not present in calculations of uniformly excited systems.

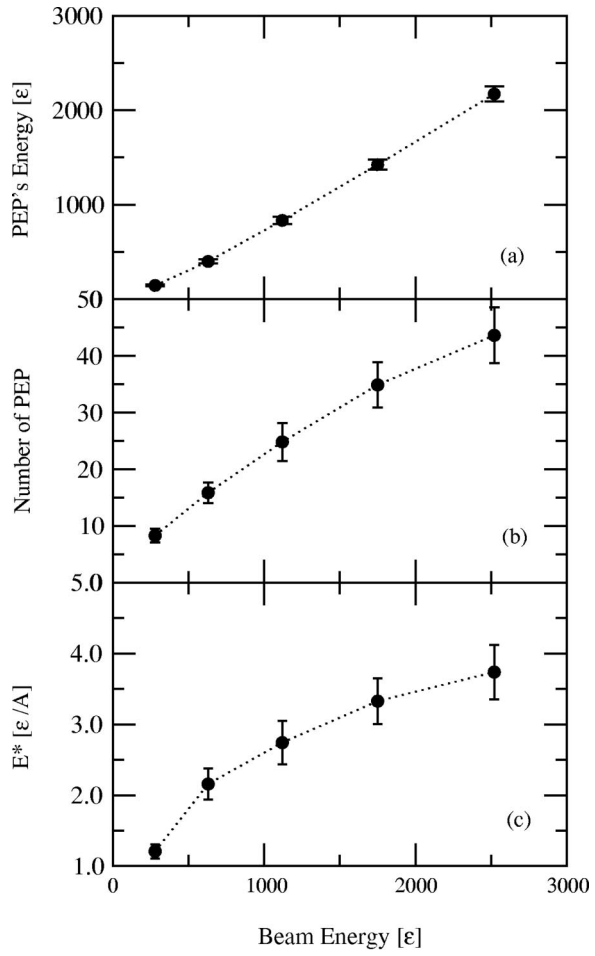

FIG. 6. The energy carried by the promptly emitted particles (a), number of PEP's produced (b), and the excitation energy per particle of the remaining system (c) as a function of the beam energy.

C. Fragment-formation time

After the *deposition* time, t_d (see Sec. III A), the energy remaining in the system is fully distributed, and the **r**-**p** density correlations induced by the initial shock wave start to build up a collective expansion. Eventually, this expansion will turn those early fluctuations into well defined fragments in **r** space making them recognizable by the MST algorithm. The caloric curve should reflect the state of the system at the phase change; here we take this time as the fragment-formation time, τ_{ff}, associated to the stabilization of the ECRA density fluctuations.

As mentioned in Sec. II B, ECRA searches for the most-bound density fluctuation (MBDF) in phase space, cf. Eq. (3); we study the stabilization of these partitions using the differential persistence coefficient, P^{dt} [cf. Eq. (6)]. Since P^{dt} is normalized to be equal to 1 when the microscopic composition of a partition at time t differs from the one at $t+dt$ by just one ''evaporated'' particle, τ_{ff} can then be defined as the earliest time when $P^{dt}(t)=1$. Figure 7 shows the temporal evolution of P^{dt} calculated using ECRA partitions from experiments with $E_{beam}=630\epsilon,1120\epsilon,1750\epsilon,$ and 2520ϵ, $dt=2t_0$, and considering only fragments of mass greater than three particles. The results obtained are τ_{ff}

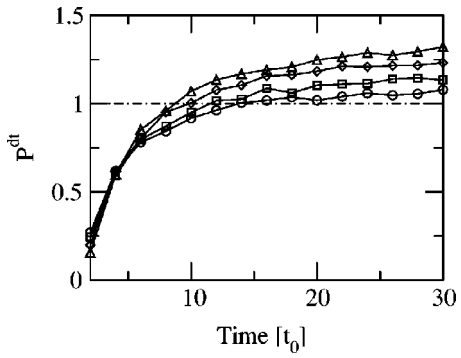

FIG. 7. Temporal dependence of the persistence coefficient calculated for collisions with $E_{beam}=630\epsilon$ (circles), 1120ϵ (squares), 1750ϵ (diamonds), and 2520ϵ (triangles), obtained using ECRA partitions and a value of $dt=2t_0$.

$=20t_0,15t_0,12t_0,$ and $10t_0$ for these energies, respectively.

The temporal evolution of the MBDF can be traced using P^+ and P^-, as done with MSTE clusters (Sec. III A). The corresponding time evolution of the forward and backward persistence coefficients for the ECRA partitions, which use correlations in **r**-**p** space, are shown in Figs. 8(a)–8(d) for collisions with beam energies of 630ϵ, 1120ϵ, 1750ϵ, and 2520ϵ, and taking $t_\infty=50t_0$. The fact that P^+ reaches the reference before P^- reflects an initial overproduction of ECRA fragments, due to the highly nonequilibrium energy injection process. However, after preequilibrium, the subsequent dynamics ''smoothes'' the density fluctuations in **r**-**p** phase space and a coalescentlike behavior for the ECRA clusters can be observed. On the other hand, similar to the results of the MSTE clusters [cf. Fig. 4(c)], an evaporative-like dynamics was observed for ECRA partitions calculated after $t\gg\tau_{ff}$, i.e., after the clusters are already formed and vary their microscopic composition only by monomer evaporation. This underlines the fact that τ_{ff} appears to be well suited to define the *fragment-formation time*.

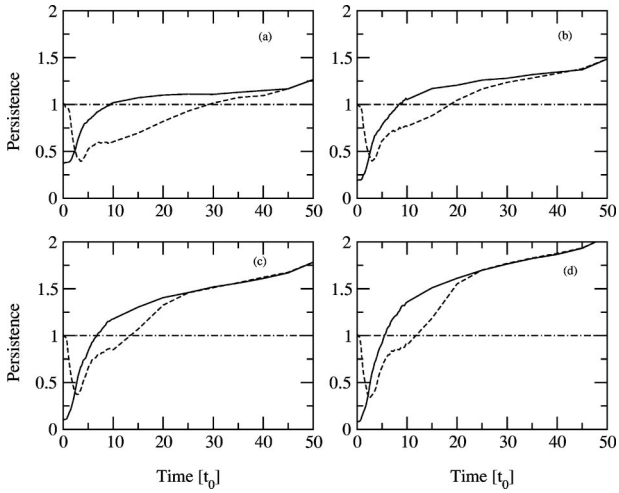

FIG. 8. Forward (solid lines) and backward (dashed lines) persistence coefficients, calculated over ECRA partitions for collisions with $E_{beam}=630\epsilon$ (a), 1120ϵ (b), 1750ϵ (c), and 2520ϵ (d). See text for details.

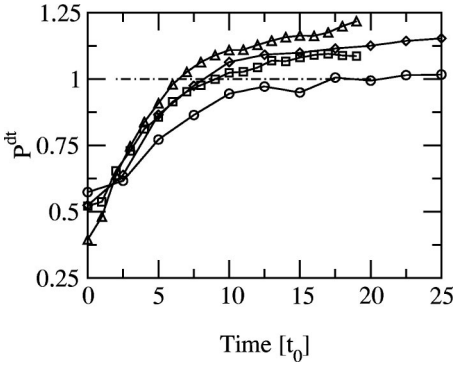

FIG. 9. Temporal dependence of the differential persistence coefficient calculated for ECRA partitions for uniformly excited systems with $E^*=2.2\epsilon$ (circles), 2.8ϵ (squares), 3.4ϵ (diamonds), and 3.8ϵ (triangles), and using a value of $dt=2t_0$.

D. Comparison to uniformly excited systems

The differences between collision-induced breakups and those produced by the addition of a uniform excitation (''*explosions*'') can be educational. To simulate this second kind of experiments 2D 100 Lennard-Jones particle drops were given random velocities according to a Maxwell-Boltzmann distribution with a variance compatible with a given excitation energies [22].

Figure 9 shows the time evolution of $P^{dt}(t)$ for ECRA partitions calculated over explosive experiments with excitation energies per particle of $2.2\epsilon, 2.8\epsilon, 3.4\epsilon$, and 3.8ϵ (corresponding to collisional events with $E_{beam}=630\epsilon$, 1120ϵ, 1750ϵ, and 2520ϵ, respectively). The fragment-formation times extracted from the figure are $\tau_{ff}=20t_0$, $12t_0$, $9t_0$, and $8t_0$ in general agreement with the corresponding times of the collisions.

On the other hand, Fig. 10 shows the forward and backward persistence coefficients, $P^+(t)$ and $P^-(t)$, for the explosive experiments considered before. Qualitative differences arise in the microscopic dynamics of the ECRA clusters when collisional events (see Fig. 8) are compared with isotropically excited systems. In the explosions, the direct persistence coefficients are always smaller than the inverse persistence ones. Moreover, as P^+ crosses the reference value after P^-, an evaporativelike behavior of the ECRA clusters can be associated for this kind of excitation in the early stage of the evolution. As mentioned above, this is not the case for collisional experiments.

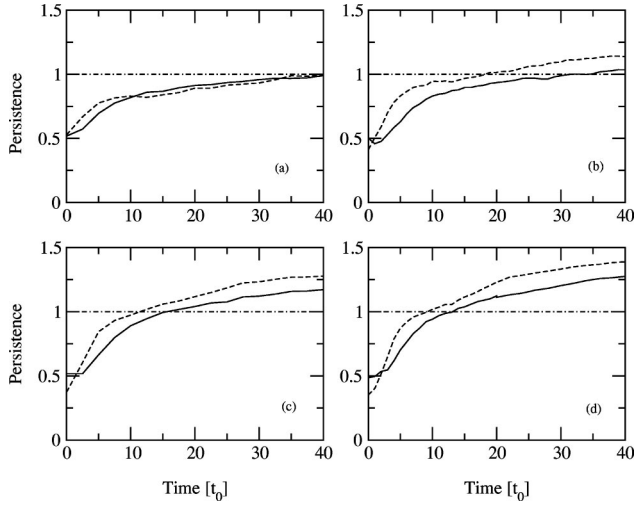

FIG. 10. Forward (solid line) and backward (dashed line) persistence coefficients, calculated for ECRA clusters for isotropically excited systems with $E^*=2.2\epsilon$ (a), 2.8ϵ (b), 3.4ϵ (c), and 3.8ϵ (d). See text for details.

The picture emerging suggests that the particle correlations in phase space have to be built from scratch in explosions. Likewise, the collective radial flux built from interparticle *disordered* collisions cools down the system leading to a microscopic stabilization of the density fluctuations (i.e., ECRA clusters). The persistence coefficients indicate that the later cluster dynamics is mainly evaporative.

Collisions, on the other hand, appear to have a two-stage development. A first stage of high momentum transfer (see Fig. 3) with a mechanical shock front produces large numbers of light ECRA clusters and internal surfaces, followed by a second stage with an isotropic collision pattern. In this second stage, the system is still dense and a coalescentlike behavior sets in enlarging the ECRA clusters and starting an expansion. This process continues until the density is lowered by this radial expansion.

Although the microscopic dynamics of the MBDF's calculated by ECRA are quite different for early times, similar fragment-formation times τ_{ff} are found for both explosions and collisions. Furthermore, the finding of stages followed by a radial expansion in the collisions appears to be in agreement with experimental observations [17].

IV. TEMPERATURE

The next step leading to the caloric curve is the calculation of the temperature of the system at fragmentation time. Since at this time the system can still be dense (cf. Sec. III A) with a temperature varying in space, two complementary measures of temperature will be used: a ''local'' temperature (using local velocity fluctuations around a local mean) and a cluster temperature (using velocity fluctuations around each cluster's mean). This appears to be justified as isotropically excited drops are known to achieve thermal equilibrium during the breakup [22]. Purists with reservations about using thermodynamic concepts for small and transient systems are referred to in Refs. [26,27]. We now define these temperatures and study their temporal evolution.

A. Local temperature

To calculate the local temperature, T_{loc}, a square grid is placed over the region of interest and the local velocity fluctuations of the particles in every cell are calculated. Formally,

$$T^i_{loc}=\tfrac{1}{2}\langle(\langle v^2\rangle_i-\langle v\rangle_i^2)\rangle_{ev}, \tag{7}$$

where v represents the particle velocities, $\langle\cdots\rangle_i$ stands for average over particles in cell i, and $\langle\cdots\rangle_{ev}$ for an average over all events. Cells are of $l_{cell}=3\sigma$ of side cells to assure approximately a mean cell population of seven particles for

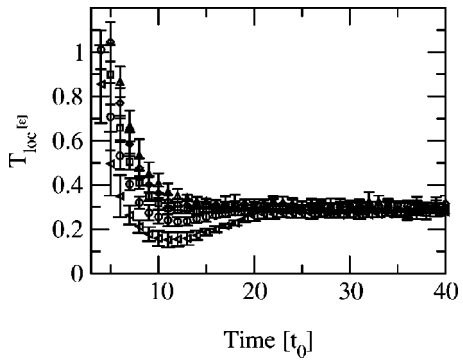

FIG. 11. Mean local temperature $\overline{T}_{loc}$ as a function of time, calculated for collisions with $E_{beam}=280\epsilon$ (left triangles), $E_{beam}=630\epsilon$ (circles), 1120ϵ (squares), 1750ϵ (diamonds), and 2520ϵ (up triangles).

$t<20t_0$. To further quantify the temperature of the central cells, the average $\overline{T}_{loc}(t)$ is calculated over central cells with a center not farther than 9σ from the center of mass of the system. Approximately 40% of the particles remains in that region for $t\leqslant 40t_0$ for the more energetic experiments.

Figure 11 shows that the system cools down rapidly until $\overline{T}_{loc}\sim 0.3\epsilon$ at $t\sim 15t_0$ for all energies considered ($280\epsilon, 630\epsilon, 1120\epsilon, 1750\epsilon$, and 2520ϵ). Note that for $E_{beam}=280\epsilon$ and 630ϵ an overcooling loop can be seen. For these less energetic collisions, the generated expansion is weak enough to allow the attractive interactions to produce a temporary increase of the system density before it breaks. This effect is suppressed for larger energies, where the expansion is much stronger.

B. Cluster temperature

A cluster-based temperature can be obtained looking at the internal kinetic energies of the ECRA fragments. The cluster temperature of a fragment C_i is defined as

$$T_{C_i}=\frac{1}{n_i}\sum_{j\in C_i} K_j^{\text{c.m.}}, \tag{8}$$

where n_i is the number of particles in cluster C_i, and $K_j^{\text{c.m.}}$ is the kinetic energy of particle j measured in the center of mass frame of the cluster to which it belongs. Figure 12 shows the typical dependence of T_C on the ECRA-cluster masses calculated in $E_{beam}=1120\epsilon$ events at $t=5,7$, and $20t_0$. Since a saturating behavior is observed for clusters with $n_i\geqslant 20$, a mean cluster temperature, T_{clus}, can be defined as the average temperature of clusters with more than 20 particles.

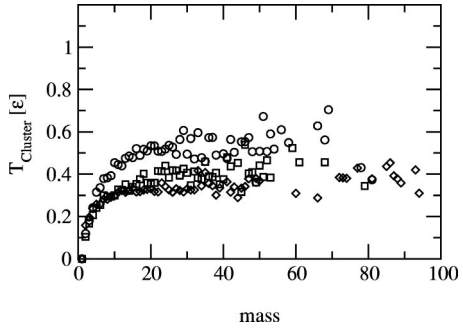

FIG. 12. Mass dependence of ECRA-cluster temperatures for collisions with $E_{beam}=1120\epsilon$ calculated at times $t=5t_0$ (circles), $t=7t_0$ (squares), and $t=20t_0$ (diamonds).

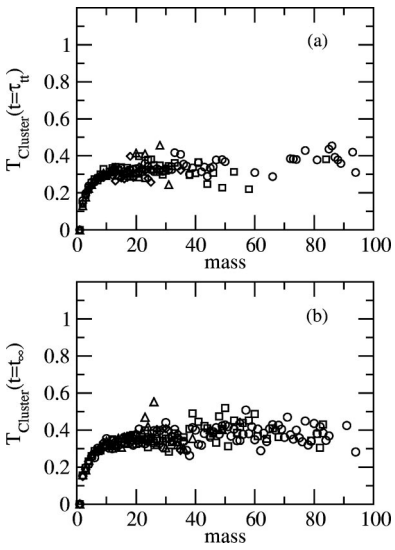

FIG. 13. Cluster temperature as a function of fragment mass, calculated for ECRA clusters at $t=\tau_{ff}$ (a), and $t=t_\infty$ (b) for collisions with $E_{beam}=630\epsilon$ (circles), 1120ϵ (squares), 1750ϵ (diamonds), and 2520ϵ (triangles).

The ECRA clusters are formed by a compromise between the maximum temperature the clusters can sustain and the cohesive effects of the pair potential interaction. Initially, the cluster constituents are close to their initial positions with large (more negative) values of the potential which permit them stand hotter temperatures. As the system evolves and the clusters become more rarefied, the potential energy increases (becomes less negative) reducing the maximum temperature the clusters can sustain. Finally, as the clusters attain their asymptotic composition, the temperature stabilizes. The shift observed in Fig. 12 at early times, $t=5t_0$, is due to the the lack of development of the radial flux.

Figures 13(a) and 13(b) show the cluster temperatures T_C at fragment-formation time, τ_{ff}, and at t_∞ for $E_{beam}=280\epsilon, 630\epsilon, 1120\epsilon, 1750\epsilon$, and 2520ϵ. At τ_{ff}, although the system is still dense (the biggest MST cluster has $\sim 90\%$ of the total mass), the cluster temperatures calculated for ECRA clusters have already achieved their asymptotic values and are in agreement with the corresponding local temperatures $\overline{T}_{loc}$. This behavior has also been found in explosivelike experiments (see Ref. [24], and references therein).

Two remarks are in order. First, it should be clear by now that the temperature of the system *at* τ_{ff} can be extracted from the estimation of the *asymptotic* cluster temperatures in both cases, collisional and explosivelike experiments. Second, it is worth noting that in our analysis we did not have to invoke any *global equilibrium* hypothesis (such as the existence of a freeze-out volume) in order to calculate the system temperature. Instead, our temperature definitions rely on a

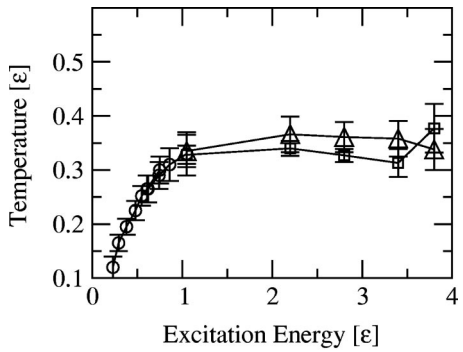

FIG. 14. Caloric curve calculated with data obtained from collisions. For low energy experiments (circles), the temperature of the biggest fragment is shown. For high energy events, the system temperature $\overline{T_{loc}}$ (squares) and the cluster temperature at fragmentation times T_{clus} (triangles) are shown.

local equilibrium scenario which seems to describe the fragmentation process in a more natural way [29].

V. CALORIC CURVE

After the simulation of the collision dynamics, the detection of PEP's and fragments, the identification of fragmentation time, and the calculation of the excitation energy and temperature, the caloric curve can finally be obtained. Formally this quantity, which has been investigated experimentally [28,13,14,16,17,7,8] and computationally [19,22,24], is the functional relationship of the system temperature with its excitation energy. In this section we will extend the analysis to collisionally excited Lennard-Jones drops.

Figure 14 shows the caloric curve calculated for a broad range of energies for collisionally excited systems. For completeness, the caloric curve for low energy experiments, $E^* < 1\epsilon$, where no fragmentation is expected, is also calculated. (Since in these experiments no particles, or just a few, are evaporated, the temperature is calculated for the larger cluster that remains after the projectile collision.) For higher excitation energies we show both the average local temperature, T_{loc}, and the cluster temperatures, T_{clus}, at $t=\tau_{ff}$.

As seen in Fig. 14, the caloric curve is similar to the one obtained for isotropically excited systems [24]. Here again, the relevant feature is the rather constant temperature behavior in the region that corresponds to the fragmentation regime and beyond. In other words, data from collisions appear to yield a ''rise-plateau'' shape for the caloric curve, without the final ''rise'' expected for the heating of a possible ''gaseous'' phase.

VI. CONCLUSIONS

As a conclusion we now answer the question asked in Sec. I, namely would the correlations induced by the collision impede the obtention of the caloric curve? The answer is an unconditional ''no.'' Even though collisions produce many PEP's and induce internal surfaces and large density correlations, the temperature information of the system at fragmentation time appears to be reflected in the cluster temperature with high fidelity. This, in conclusion, makes collisions a useful tool to explore the caloric curve of fragmenting systems, provided the excitation energy responsible for the fragmentation process is properly calculated. Work in progress is developing a more realistic MD model to identify participant nucleons and their excitation energy kinematically in nuclear collisions.

ACKNOWLEDGMENTS

This work was supported by the National Science Foundation (PHY-96-00038), the Universidad de Buenos Aires (EX-070), and CONICET. J.A.L. acknowledges the hospitality of the Universidad de Buenos Aires.

[1] P. F. Mastinu *et al.*, Phys. Rev. Lett. **76**, 2646 (1996).
[2] J. A. Blink and W. G. Hoover, Phys. Rev. A **32**, 1027 (1985).
[3] K. Bomann *et al.*, Science **274**, 5278 (1996); **274**, 956 (1996).
[4] J. E. Finn *et al.*, Phys. Rev. Lett. **49**, 1321 (1982).
[5] N. T. Porile *et al.*, Phys. Rev. C **39**, 1914 (1989).
[6] X. Campi, H. Krivine, and E. Plagnol, Phys. Rev. C **50**, R2680 (1994).
[7] J. Pochodzalla, Prog. Part. Nucl. Phys. **39**, 43 (1997).
[8] H. Feldmeier *et al., Gross Properties of Nuclei and Nuclear Excitations* (GSI, Darmstadt, Germany, 1999).
[9] *Isospin Physics in Heavy Ion Collisions at Intermediate Energies*, edited by B.-A. Li and W. U. Schröder (Nova, New York, 2001).
[10] J. B. Natowitz *et al.*, Phys. Rev. C **52**, R2322 (1995).
[11] X. Campi, H. Krivine, and E. Plagnol, Phys. Lett. B **385**, 1 (1996).
[12] V. Viola *et al.*, Phys. Rev. C **59**, 2660 (1999).
[13] J. Pochodzalla *et al.*, Phys. Rev. Lett. **75**, 1040 (1995).
[14] V. Serfling *et al.*, Phys. Rev. Lett. **80**, 3928 (1998).
[15] K. Hagel *et al.*, Phys. Rev. C **62**, 034607 (2000).
[16] J. A. Hauger *et al.*, Phys. Rev. Lett. **77**, 235 (1996).
[17] J. A. Hauger *et al.*, Phys. Rev. C **57**, 764 (1998).
[18] G. Papp and W. Nörenberg, Heavy Ion Phys. **1**, 241 (1995).
[19] Y. Sugawa and H. Horiuchi, Phys. Rev. C **60**, 064607 (1999).
[20] A. Barrañón *et al.*, Rev. Mex. Fis. **45-Supplement 2**, 110 (1999).
[21] R. Donangelo and S. R. Souza, Phys. Rev. C **52**, 326 (1995).
[22] A. Strachan and C. O. Dorso, Phys. Rev. C **55**, 775 (1997).
[23] C. O. Dorso and J. Randrup, Phys. Lett. B **301**, 328 (1993).
[24] A. Strachan and C. O. Dorso, Phys. Rev. C **58**, R632 (1998).
[25] A. Strachan and C. O. Dorso, Phys. Rev. C **59**, 285 (1999).
[26] P. Labastie and R. Whetten, Phys. Rev. Lett. **65**, 1567 (1990).
[27] Terrell L. Hill, *Thermodynamics of Small Systems*, (Dover, New York, 1994).
[28] J. Pochodzalla *et al.*, Nucl. Phys. **A583**, 553c (1995).
[29] A. Chernomoretz *et al.*, Phys. Rev. C **64**, 024606 (2001).